 doi:10.20944/preprints201910.0202.v1

Sea level rise scenario for 2100 A.D. in the heritage site of Pyrgi (Santa Severa, Italy)

Marco Anzidei[1], Fawzi Doumaz[1], Antonio Vecchio[2-3] Enrico Serpelloni[1], Luca Pizzimenti[1], Riccardo Civico[1] and Flavio Enei[4]

[1] Istituto Nazionale di Geofisica e Vulcanologia, Italy

[2] Radboud Radio Lab, Department of Astrophysics/IMAPP, Radboud University - Nijmegen, The Netherlands

[3] Lesia Observatoire de Paris, PSL Research University, Paris, France

[4] Museo del Mare e della Navigazione Antica, Santa Severa, Italy

Abstract

Sea level rise is one of the main factor of risk for the preservation of cultural heritage sites located along the coasts of the Mediterranean basin. Coastal retreat, erosion and storm surges are yet posing serious threats to archaeological and historical structures built along the coastal zones of this region. In order to assess the coastal changes by the end of 2100 under an expected sea level rise of about 1 m, a detailed determination of the current coastline position and the availability of high resolution DSM, is needed. This paper focuses on the use of very high-resolution UAV imagery for the generation of ultra-high resolution mapping of the coastal archaeological area of Pyrgi, near Rome (Italy). The processing of the UAV imagery resulted in the generation of a DSM and an orthophoto, with an accuracy of 1.94 cm/pixel. The integration of topographic data with two sea level rise projections in the IPCC AR5 2.6 and 8.5 climatic scenarios for this area of the Mediterranean, were used to map sea level rise scenarios for 2050 and 2100. The effects of the Vertical Land Motion (VLM) as estimated from two nearby continuous GPS stations located as much as close to the coastline, were included in the analysis. Relative sea level rise projections provide values at 0.30±0.15 cm by 2050 and 0.56±0.22 by 2100, for the IPCC AR5 8.5 scenarios and at 0.13±0.05 cm by 2050 and 0.17±0.22 by 2100, for the IPCC AR5 2.6 scenario. These values of rise will correspond to a potential beach loss between 12.6% and 23.5% in 2100 for RCP 2.6 and 8.5 scenarios, respectively, while during the highest tides the beach will be reduced up to 46.4%. With these sea level rise scenarios, Pyrgi with its nearby Etruscan temples and the medieval castle of Santa Severa will be soon exposed to high risk of marine flooding, especially during storm surges, thus requiring suitable adaptation strategies.

Key words: Sea level rise, coastlines, 2100, heritage sites, Pyrgi, Mediterranean, UAV, DSM

1. Introduction

Observational and instrumental data collected worldwide since the last two-three centuries show that global sea level is continuously rising with an accelerated trend in recent years, in coincidence with the rise of global temperatures [1]. Global mean sea level is expected to rise in the range of about 75-200 cm by 2100 (www.ipcc.ch) [2, 3], representing among the most serious effects of climate change to face in the next decades. These values will be even larger in subsiding coasts of the Mediterranean, entailing widespread environmental

Preprints (www.preprints.org) | NOT PEER-REVIEWED | Posted: 17 October 2019 doi:10.20944/preprints201910.0202.v1

changes, coastal retreat, marine flooding and loss of land, which will be subtracted to human activities. Sea level rise will amplify the impacts exerted by a multitude of hazards (i.e. storm surges, flooding, coastal erosion and tsunamis) on infrastructure and building integrity, people safety, economic assets and cultural heritage.
Therefore, it is important to mitigate these risks by providing multi-temporal scenarios of expected inland extension of marine flooding in consequence of sea level rise, for a cognizant coastal management.
This is particularly important for the Mediterranean region where ancient civilizations were born and developed along its coasts. For the above reasons, a large number of heritage sites are located at the waterfront or very close to the sea level and are yet exposed to marine flooding under the effects of the ongoing climate change. A large part of these sites, which are dated back to the Greek, Roman and Medieval ages, are exposed at increasing risks from coastal hazards related to sea-level rise.
In this study we show an effective application for the coastal archaeological area of Pyrgi, near Rome (Italy) (Fig.1). Aerial photogrammetric surveys performed by small Unmanned Aerial Vehicles (UAVs), provided an accurate beach topography at low costs and in short time. Results, have been analyzed in combination with climatic projections and vertical land movements (VLM), to support the realization of expected sea-level rise scenarios.
The proposed methodology can be exported in any other areas of the Mediterranean region and beyond, supporting policy makers to identify the best adaptation strategies toward sea level rise impacts and to protect heritage sites.

2. Geo-archaeological setting

The heritage site of Pyrgi is located along the coasts of northern Latium, between the villages of Santa Severa and Cerveteri, about 50 km north of Rome (Italy) (Fig.1). This area includes the Castle of Santa Severa that with Pyrgi, is one of the most important heritage sites of the Tyrrhenian coast. The area has been settled since the V-IV millennium B.C. [4] and continuously developed during the Neolithic (V.IV millennium B.C.), in the Bronze Age (II millennium B.C.) and in the Iron Age (IX-VIII century B.C.), thanks to its good environmental conditions. In the Etruscan phase (VII-VI century B.C.), Pyrgi played an important role in the maritime commerce and its well-known port was frequented by Greeks and Phoenicians ships. The area includes a sanctuary and the temples of Eileithyia-Leukothea and Apollo, the Etruscan Uni analogue to the Phoenician Astarte [4].
With the Romanization of this area (III century B.C.), Pyrgi became a maritime colony and a tall fortress surrounded by a polygonal wall was built on part of the Etruscan settlement. This fortress continued to be used until the V-VI century A.D. when it was transformed into an imperial villa. Later, the medieval and renaissance village became a large farm located between the main harbors of Rome and Civitavecchia [4, 5, 6, 7].
Concerning the geological setting, the coast of Pyrgi belongs to the roman co-magmatic province [8] that underwent to major volcanic activity during the Plio-Pleistocene. The surface geology is characterized by a bedrock belonging to the allochthonous Outer Ligurids [9], represented by the Tolfa Formation, spanning from the Late Cretaceous to Palaeogene [10], or the Pietraforte formation [11]. The latter consists in a series of marl limestone and grey marl beds partly buried by biogenic sandstone of the Early-Middle Pleistocene Panchina Formation [12].
The Holocene deposits are represented by travertines, slope debris, alluvial, weathering deposits, gravels and sandy beaches [13]. The neotectonics of this area is highlighted by the MIS 5.5 marine terraces that show an overall weak uplift of the inland sector for the last 124.000 years [14; 15], likely related to magmatic injections under the Vulsini and Sabatini

Preprints (www.preprints.org) | NOT PEER-REVIEWED | Posted: 17 October 2019 doi:10.20944/preprints201910.0202.v1

volcanic complexes [8]. Anyway [16] underline that the long term uplift may not be appropriate for the past two millennia, when some weak subsidence may have occurred along the coast of Pyrgi.

3. Method

We applied a multidisciplinary approach using coastal topography, geodesy and climatic driven estimates of sea-level rise to provide maps of flooding scenarios to the year 2100 A.D. for the coast of Pyrgi. Our approach consists in three main steps: 1) the realization of UAV surveys to obtain an ultra-high-resolution orthophoto, a DSM model of the coastal area and to map the current and the projected coastline positions; 2) to estimate the current vertical land movements from the analysis of geodetic data from the nearest GPS stations; 3) by combining these data with the regional IPCC-AR5 projections (RCP-2.6 and RCP-8.5 scenarios), the upper bounds of the expected sea levels for the targeted epochs of 2050 and 2100 A.D. and the corresponding expected inland extent of the marine flooding and shoreline positions, were calculated.

4. Digital Terrain Model reconstruction

To realize the ultra-high resolution Digital Surface Model (DSM), an aerial photogrammetric survey was performed using a radio-controlled multi-rotor DJI Phantom 4pro UAV system, equipped with a high resolution lightweight digital camera, to capture a set of aerial images of the investigated area (Tab.1).

The UAV was controlled by an autopilot system using waypoints previously planned by PIX4D® capture IOs App as a Ground Control Station system. To optimize the photogrammetric spatial resolution and coverage of the surveyed area, a constant altitude of 70 m was maintained during the flight and 306 partly overlapping (70% of longitudinal and 70% lateral overlapping between subsequent photos), aerial digital photos were acquired during three successful flights of a few minutes of duration each. To scale the aerial images, we used a dual-frequency geodetic GPS/RTK receiver STONEX S900A® to measure the coordinates of a set of reference Ground Control Points (GCPs) falling in the investigated areas. GCPs positions were estimated in real time by the RTK technique with about 1–2 cm accuracy, with respect to the reference GPS station TOLF belonging to the GNSS network of the INGV [17] and also pertaining to the ITALPOS network (https://hxgnsmartnet.com/en-gb/) for real time positioning services. We used the Agisoft PhotoScan® software package (http://www.agisoft.com) based on the Structure-from-Motion photogrammetry technique [18] to process the acquired georeferenced images. The analysis included: 1) camera alignment with image position and orientation; 2) generation of a dense points cloud and 3) generation of an orthophoto covering a land surface of 0.226 km^2 with a ground resolution of 1.94 cm/pixel and the DSM creation in the WGS84-UTM32 coordinate system.

The obtained ortho-rectified images (orthophotos) and digital elevation models were also managed by Global Mapper® and ESRI ArcGis® software to create cross sections, slope maps, surfaces, coastline positions and calculate the dimension of the potential flooded areas. The extracted Digital Surface Model has a resolution of 15.5 cm/pixel and a point density of 41.5 points/$m^{2.}$

As targets for GCPs measured by GPS/RTK we used a set of: i) natural markers belonging to fixed structures (e.g. the center of manholes, wall and sidewalk corners, small structures or large stones); and ii) mobile targets for the time of the flight, such as thin metal crosses

of 60x60 cm of size, deployed in the investigated area. All these GCPs were chosen to be easily recognizable on the images during data analysis.

In total, 22 Ground Control Points (GCPs) and Check Points (CPs) were used to georeference the orthophoto with the ground control point toolset of AGISOFT photoscan (Fig.2). The 3D coordinates of these points have been estimated with a mean RMS of 0.6 and 0.9 cm for the horizontal and vertical components, respectively, and were used to evaluate the vertical accuracy of our final DSM. In Fig.2 is reported the orthophoto, while the DSM is shown in Fig.3.

5. Tidal correction and coastline position

The coast of Pyrgi, like most of the coasts of the Mediterranean Sea, is characterized by a micro-tidal environment and the tides are generally in the range of ±30 cm. Only in the Gulf of Gabes (Tunisia) and the North Adriatic Sea (Italy), tides may reach amplitudes up to ~2 m [19; 20; 21; 22]. We used the tidal data collected by the Italian tidal network managed by ISPRA (www.mareografico.it) at the sea level station of Civitavecchia (located at LAT 42° 05' 38.25''; LON 11° 47' 22.73'), which is located nearby Pyrgi (Fig.1), to estimate the tide level and the local mean sea level at the time of the UAV surveys. This tide gauge station shows a valid recording period of about 8 years (2011-2019), with a sea level trend of 0.25± 0.1 mm/a, calculated from a linear fit on the monthly data (Fig.4 a). From the data analysis, a mean tide amplitude of ~35 cm and a maximum tidal range up ~60 cm has been estimated (Fig. 4 b). To define a reference level for elevation data, we used the mean sea level value for the year 2018 at the Civitavecchia tide gauge, which correspond to a level of 4.8±11.8 cm above the topographic benchmark, as estimated from the hourly tidal data. Because the UAV surveys have been performed during a high tide of 4 cm, as shown by the tidal recordings (www.mareografco.it), then the reference sea level for April 26, 2019 at 07:30 (05:30 UTC) corresponds to a position of only 0.8 cm above the mean sea level for 2018. The International Service for the Geoid - ISG (http://www.isgeoid.polimi.it/Geoid/Europe/Italy/ITG2009_g.html) [23] provides a geoid height for Pyrgi (located at Lat 42.015407 N, Lon 11.956994,E) at 48.319 m, that differs from the GPS elevation data acquired during surveys at a point along the shore placed at the sea level. This elevation value corresponds to the coastline imaged during UAV surveys and to the contour line placed at the orthometric height equal to zero represented by the elevation at -0.42 m in the DSM.

6. Vertical Land Motion (VLM) at Pyrgi

The current rate of VLM at Pyrgi was estimated by the analysis of the available GPS data collected at the nearest GNSS stations of TOLF, belonging the INGV RING network (DOI:10.13127/RING) and MAR8, belonging to the Topcon-NetGeo network (http://www.netgeo.it). These stations are located at ~6.5 km and 0.3 km of distance from the study site, respectively (Fig.1). Both these stations have a robust time series that span for 2004-2019 for TOLF (about 15 years) and 2012-2019 for MAR8 (about 7 years), respectively (Fig.5).

The GPS data analysis has been carried out following the procedures already described in [24] and updated in [25] adopting a three-step procedure using the GAMIT/GLOBK V10.7 (Herring et al., 2015) and QOCA software. This is part of a continental-scale GPS solution, including >3000 stations [26]. The daily positions of TOLF and MAR8 have been estimated in the GPS realization of the ITRF2008 frame [27] i.e., the IGb08 reference. The position time series have been analyzed in order to estimate, and correct, offsets due to stations

Preprints (www.preprints.org) | NOT PEER-REVIEWED | Posted: 17 October 2019 doi:10.20944/preprints201910.0202.v1

equipment changes, while simultaneously estimating annual and semi-annual periodic signals and a linear velocity term, whereas velocity uncertainties have been estimated adopting a power law + white noise stochastic model, as in [28]. The results show that both sites are relatively stable in the IGb08 reference frame, with a vertical velocity of -0.061±0.135 mm/yr for TOLF and -0.456±0.344 mm/yr for MAR8.
The tectonic stability of this region is inferred from the low level of seismicity from historical data [29] and instrumental recordings of earthquakes (www.ingv.it), which do not report the occurrence of significant events for the last 3000 years BP.
Finally, assuming the area is characterized by a limited tectonic activity, then the contribution of VLM to the local sea level rise projections for 2100 AD can be neglected in the analysis of the flooding scenarios.

7. Relative sea‑level rise projections and flooding scenarios for 2050 and 2100 A.D. at Pyrgi

To estimate the sea-level rise for 2050 and 2100 A.D. at Pyrgi, we referred to the regional IPCC AR5 sea-level projections discussed in the Fifth Assessment Report of the IPCC-AR5 (www.ipcc.ch) (data available from the Integrated Climate data Center-ICDC of the University of Hamburg, http://icdc.cen.uni hamburg.de/1/daten/ocean/ar5-slr.html). These data consist of the sea-level ensemble mean values and upper/lower 90% confidence bounds of the sea level, on a global grid (spatial resolution $1^{\circ}\times1^{\circ}$), obtained by adding the contributions of several geophysical sources driving long term sea-level changes: 1) the thermosteric/dynamic contribution (from 21 CMIP5 coupled atmosphere-ocean general circulation models AOGCMs), 2) the surface mass balance and dynamic ice sheet contributions from Greenland and Antarctica, 3) the glacier and land water storage contributions, 4) the glacial isostatic adjustment (GIA), and 5) the inverse barometer effect [1]. Projections, based on two different Representative Concentration Pathways RCP 2.6 and RCP 8.5, providing the least and most amounts of future sea level rise respectively, were used. The IPCC regional sea-level rate at the grid point closest to the location of the tide gauge station (Civitavecchia) was considered. By accounting for VLM from GPS data, very high-resolution DSM and regional IPCC sea level projections at the grid point corresponding to the investigated area, the first marine flooding scenarios for Pyrgi for 2050 and 2100 A.D have been realized. To include the VLM effect in sea-level projections, we substituted the modelled GIA contribution to the IPCC rates with the measured GPS vertical rates which includes both GIA and tectonic components, of both natural and anthropogenic origin. Uncertainties for the sea-level estimations were calculated by combining lower and upper sea level bounds from IPCC projection and errors from GPS measurements. The relative sea-level rise in RCP2.6 and RCP8.5 scenarios at 2050 and 2100 A.D. with respect to the chosen reference epoch 2017, are shown in Fig.6, and numerical values are reported in Table 2.

The projected coastline positions for 2100 A.D., corresponding to the RCP2.6 and RCP8.5 scenarios, are obtained from the DSM for the sea levels listed in Table 2 and shown in Fig.7. The computed and the represented scenarios correspond to the local mean sea level, neglecting the periodical contribution due to diurnal and semidiurnal tides. To account for it, in order to estimate the maximum inundation scenarios, the time series of daily hydrometric sea levels at Civitavecchia tidal station from January 2010 to December 2018 were included

Preprints (www.preprints.org) | NOT PEER-REVIEWED | Posted: 17 October 2019 doi:10.20944/preprints201910.0202.v1

in the analysis. The average half amplitude of daily tides was estimated as high as ~30 cm (Fig.4b). Consequently, in the RCP 8.5 scenario for 2100, taking into account both the sea-level rise (56 cm) and the mean daily tides (30 cm), we can infer a maximum water level of 86 cm. Because high tides may reach 45 cm for a few hours a year (Fig.4b), the maximum expected water level may reach up to 101 cm above the current level.
For the RCP 2.6 scenario for 2100, considering a sea-level rise of 30 cm and the same mean daily tides (30 cm), a maximum sea-level rise of 60 cm can be inferred. During the rare maximum highest tides (45 cm) (Fig.4 b), the maximum expected water level would reach 75 cm above the 2019 level.
With these sea levels projections for 2100 A.D., the nearby beaches will be largely flooded, as well as the coast surrounding the castle. Although the Temple of Pyrgi is partially protected from the sea by sandy dunes, it will likely undergo to water intrusion and frequent flooding, especially during storm surges (Figs.7, 8). In Fig.8 and 9 are reported four cross sections traced normal to the coast and across the archaeological area of Pyrgi. Although south of the castle the dune system facing the beach is protecting the temples, the sea level rise by 2100 A.D. will likely cause an expected beach retreat up to 10 m, as argued from the cross sections B, C, D in Figs 7 and 8. While the beach facing the north-west side of the castle, which is unprotected by the dune system, will likely undergo to a retreat up to 25 m (cross section A), exposing the castle to erosion and flooding.
Finally, in Tab.3 are reported the expected flooded areas in 2050 and 2100 A.D. for the RCP 8.5 and RCP 2.6 climatic scenarios, together with the corresponding percentage of beach loss, which may reach up to 46% during the highest tides.

8 Discussion and conclusions

In this study, we assessed the marine flooding scenarios for 2050 and 2100 for the relevant heritage sites of Pyrgi, on the basis of a high-resolution DSM, rates of VLM from GPS data, tidal data from the nearby tide gauge and the RCP 2.6 and 8.5 climatic scenarios released by the IPCC. The result of this study highlights the flooding impacts on the beach and the archaeological zones with a potential local sea-level rise for the IPCC 8.5 scenario of about 56 cm for 2100 A.D. that would reach more than 86 cm and up to 101 cm during the highest tides, as estimated by the value of the half amplitude frequency of the daily tides. In addition, if we consider that 2000 year ago, during the roman time, the shoreline was placed at about 1.2 m below the current sea level, as estimated by the fish tank data [29], a continuous sea level rise is occurring since the I century A.D. with an acceleration that started about 100±53 years ago, at the beginning of the Industrial Era [16]. Due to the potential significant impacts on both the coast and the heritage sites of the Temple of Pyrgi and the Santa Severa Castle with a beach retreat up to ~25 m, the expected scenario shown in this study can support adaptation planning at different time scales, in agreement with the Protocol on Integrated Coastal Zone Management (ICZM) in the Mediterranean. Our results details previous studies for the Italian [19, 30, 31, 32, 33, 34, 35] and the Mediterranean [36, 37] regions and can raise awareness of policymakers and heritage managers, highlighting the need for adaptation actions to protect Pyrgi from marine flooding and erosion under the current conditions and for the expected sea level rise scenarios. To this regard, we remark that [38] estimated a mean coastal erosion at a rate of 3.3 cm/year since the last 2.500 years although the retreat of the soft cliffs characterizing the Pyrgi coastline is occurring mostly during high energy marine events.
Finally, although the role and effects of waves on the marine flooding are out of the scope of this study, we remark that storm waves approaching the coast from the Northwest, West and Southwest marine sectors are particularly dangerous for Pyrgi. The waves approaching to the coast with fetches even of some hundreds of km long are weakly slowed down by the

seafloor morphology, resulting in a potential increasing of wave energy in a sea level rise condition [39] thus leading to increasing coastal erosion and potential enhanced damages to the heritage site, posing problems for its future preservation.

Acknowledgements

This study has been partially supported by the SAVEMEDCOASTS Project, funded by the EU (Agreement Number: ECHO/SUB/2016/742473/PREV16, coordinator Marco Anzidei). We are thankful to Vincenzo Sepe of the INGV, for his support during preliminary GPS/RTK surveys.

References

1. Church, J. A.; Clark, P. U.; Cazenave, A.; Gregory, J. M.; Jevrejeva, S.; Levermann, A.; Merrifield, M.A.; Milne, G.A.; Nerem, R.S.; Nunn, P.D.; Payne, A.J.; Pfeffer, W. T.; Stammer, D.; Unnikrishnan, A.S. Sea-level rise by 2100. Science, 2013b, 342, 1445–1445.

2. Bamber, J.L.; Oppenheimer, M.; Koppd, R.E.; Aspinallf, W.P.; Cooke, R.M. 2019. Ice sheet contributions to future sea-level rise from structured expert judgment. www.pnas.org/cgi/doi/10.1073/pnas.1817205116

3. Veermer, M.; Rahmstorf, S. Global sea level linked to global temperature. PNAS, 2009, 106, 21527–21532.

4. Enei, F. Santa Severa tra leggenda e realtà storica. Pyrgi e il Castello di Santa Severa alla luce delle recenti scoperte, Grotte di Castro 2013, 1-413.

5. Colonna, G. Il santuario di Pyrgi dalle origini mitistoriche agli altorilievi frontonali dei Sette e di Leucotea. Scienze dell'Antichità, Poligrafico dello Stato, Roma. 2000.

6. Enei, F. Pyrgi Sommersa. Ricognizioni archeologiche subacquee nel porto dell'antica Caere. *Museo civico Santa Marinella*, Santa Marinella *2008, 1-115*

7. Enei, F. Dal sito di Pyrgi, antico porto di Caere, nuovi dati per lo studio della linea di costa di epoca etrusca, *Archaeologia Maritima Mediterranea*, 10, Serra Editore, Pisa 2013, 165-176

8. Mattei, M.; Conticelli, S.; Giordano, G. The Tyrrhenian margin geological setting: from the Apennine orogeny to the K-rich volcanism. In Funiciello, R. & Giordano, G. (eds) The Colli Albani Volcano. Special Publications of IAVCEI, 3, 7–27. 2009, Geological Society, London

9. Sestini, G.; Bruni, P.; Sagri, M. The flysch basins of the Northern Apennines: a review of facies and of Cretaceous-Neogene evolution. Memorie della Società Geologica Italiana 1986, 31, 87-106.

10. Abbate, E.; Sagri, M. The eugeosynclinal sequences. In: Sestini, G. (Ed.), Development of the Northern Apennines Geosyncline. Sedimentary Geology 1970, 4, 251-340.

11. Alberti, A.; Bertini, M.; Del Bono, G.L.; Nappi, G.; Salvati, L. Note illustrative della Carta Geologica d'Italia alla scala 1: 100000. Tuscania-Civitavecchia Fogli 136-142. Poligrafica & Cartevalori, Ercolano (Napoli), 1970.

12. Chiocchini, U.; Gisotti, G.; Macioce, A.; Manna, F.; Bolasco, A.; Lucarini, C.; Patrizi, G.M. Environmental geology problems in the Tyrrhenian coastal area of Santa Marinella, Province of Rome, central Italy. Environmental Geology 1997, 32 (1), 1-8.

13. Ferranti, L.; Antonioli, F.; Mauz, B.; Amorosi, A.; Dai Pra, G.; Mastronuzzi, G.; Monaco, C.; Orrù, P.; Pappalardo, M.; Radtke, U.; Renda, P.; Romano, P.; Sansò, P.; Verrubbi, V. Markers of the last interglacial sea-level high stand along the coast of Italy: tectonic implications. Quaternary International 2006, 145-146, 30-54

14. Ferranti, L.; Antonioli, F.; Anzidei,M.; Monaco, C.; Stocchi, P. The timescale and spatial extent of vertical tectonic motions in Italy: Insights from coastal tectonic studies. Rendiconti Online Societa Geologica Italiana, 2010, 11(2), 683 – 684.

15. Karner, D.; Marra, F.; Florindo, F.; Boschi, E. Pulsed uplift estimated from terrace elevations in the coast of Rome: evidence for a new phase of volcanic activity? *Earth and Planetary Science Letters* **2001**, 188, 135-148.

16. Lambeck, K.; Anzidei M.; Antonioli, F.; Benini, A., Esposito, A. Sea level in Roman time in the Central Mediterranean and implications for recent change. Earth Pla. Sci. Lett. 2004, 224(3–4):563–575

17. Avallone, A.; Selvaggi, G.; D'Anastasio, E.; D'Agostino, N.; Pietrantonio, G.; Riguzzi, F.; Serpelloni, E.; Anzidei, M.; Casula, G.; Cecere, G.; D'Ambrosio, C.; De Martino, P.; Devoti, R.; Falco, L.; Mattia, M.; Rossi, M.; Obrizzo, F.; Tammaro, U.; Zarrilli, L. The RING network: improvement of a GPS velocity field in the central Mediterranean. Annals of Geophysics, 2010, 53 (2), 39-54.

18. Ullman, S. The interpretation of structure from motion. *Proc. Royal Society of London Ser. B,* **1979**, 203, 405–426

19. Antonioli, F.; Anzidei, M.; Amorosi, A.; Lo Presti, V.; Mastronuzzi, G.; Deiana, G.; De Falco, G.; Fontana, A.; Fontolan, G.; Lisco, S.; Marsico, A.; Moretti, M.; Orrù, P.; Sannino, G.; Serpelloni, E.; Vecchio, A. Sea-level rise and potential drowning of the Italian coastal plains: Flooding risk scenarios for 2100. *Quat. Sci. Rev*. **2017**, 158:29–43. https://doi.org/10.1016/j.quascirev.2016.12.021

20. Sammari, C.; Koutitonsky, V.G.; Moussa, M. Sea level variability and tidal resonance in the Gulf of Gabes, Tunisia. Continental Shelf Research, 26, 2006, pp. 338-350. https://doi.org/10.1016/j.quaint.2010.03.018

21. Lambeck, K.; Woodroffe, C.D.; Antonioli, F.; Anzidei, M.; Geherls, W.R.; Laborel, J. and Wright, A. Palaeoenvironmental records, geophysical modelling and reconstruction of sea-level trends and variability on centennial and longer time scales. In *Understanding sea level rise and variability,* **2010**. Wiley-Blackwell, pp. 61-121

22. Antonioli, F.; Lo Presti, V.; Anzidei, M.; Deiana, G.; de Sabata, E.; Ferranti, L.; Furlani, S.; Mastronuzzi G.; Orru, P. E.; Pagliarulo, R.; Rovere, A.; Sannino, G.; Sansò, P.; Scicchitano, G.; Spampinato, C. R.; Vacchi, M.; Vecchio, A.; 2015. Tidal notches in Mediterranean Sea: a comprehensive analysis *Quat. Sci. Rev.* 119, 66–84. https://doi.org/10.1016/j.earscirev.2018.06.017

23. Corchete, V. The high-resolution gravimetric geoid of Italy: ITG2009. *Jou. of African Earth Sci.* **2010**, 58, 580-584.

24. Serpelloni, E.; Faccenna, C.; Spada, G.; Dong, D.; Williams, S.D.P. Vertical GPS ground motion rates in the Euro-Mediterranean region: New evidence of velocity gradients at different spatial scales along the Nubia-Eurasia plate boundary. Journal of Geophysical Research: Solid Earth, 2013, 118 (11), 6003-6024, https://doi.org/10.1002/2013JB010102

25. Serpelloni, E.; Pintori, F.; Gualandi, A.; Scoccimarro, E.; Cavaliere, A.; Anderlini, L.; Belardinelli, M.E.; Todesco, M. Hydrologically Induced Karst Deformation: Insights From GPS Measurements in the Adria-Eurasia Plate Boundary Zone. Journal of Geophysical Research: Solid Earth 123 (5), 4413-4430, https://doi.org/10.1002/2017JB015252

26. Herring, T.; King, R. W.; McClusky, S. 2010. GAMIT Reference Manual, Release 10.4. Massachussetts Institute of Technology, Cambridge, MA.

27. Devoti, R.; D'Agostino, N.; Serpelloni, E.; Pietrantonio, G.; Riguzzi, F.; Avallone, A.; Cavaliere, A.; Cheloni, D.; Cecere, G.; D'Ambrosio, C.; Falco, L.; Selvaggi, G.; Métois, M.; Esposito, A.; Sepe, V.; Galvani, A.; Anzidei, M.; The mediterranean crustal motion map compiled at INGV. *Ann Geophys*. **2017**, doi:10.4401/ag-7059.

28. Altamimi, Z.; Collilieux, X.; Métivier, L. ITRF2008: an improved solution of the international terrestrial reference frame, *J. Geod.* **2011**, 85: 457.

29. Guidoboni, E.; Comastri, A.; Traina, G. Catalogue of Ancient Earthquakes in the Mediterranean Area Up to the 10th Century. Istituto Nazionale di Geofisica, Roma, **1994**.

30. Lambeck K.; Anzidei M.; Antonioli F.; Benini A.; Verrubbi V. Tyrrhenian sea level at 2000 BP: evidence from Roman age fish tanks and their geological calibration. *Rend. Fis. Acc. Lincei* **2018**, 29(1):69–80. https://doi.org/10.1007/s1221 0-018-0715-6

31. Lambeck, K.; Antonioli, F.; Anzidei, M.; Ferranti, L.; Leoni, G.; Scicchitano, G. and Silenzi, S. Sea level change along the Italian coast during the Holocene and projections for the future. *Quat. Int.* **2011**, 232(1–2):250–257. https://doi.org/10.1016/j.quain t.2010.04.026

32. Anzidei, M.; Bosman, A.; Carluccio, R.; Casalbore, D.; D'Ajello Caracciolo, F.; Esposito, A.; Nicolosi, I.; Pietrantonio, G.; Vecchio, A.; Carmisciano, C.; Chiappini, M.; Chiocci, F.L.; Muccini, F.; Sepe, V. Flooding scenarios due to land subsidence and sea-level rise: a case study for Lipari Island (Italy). *Terra Nova* **2017**, 29(1):44–51, https://doi.org/10.1111/ter.12246

33. Anzidei, M.; Scicchitano, G.; Tarascio, S.; De Guidi, G.; Monaco, C.; Barreca, G.; Mazza, G.; Serpelloni, E.; Vecchio, A. Coastal retreat and marine flooding scenario for 2100: a case study along the coast of Maddalena Peninsula (southeastern Sicily). *Geogr. Fis. Dinam. Quat*. 41, **2018**, 5-16, DOI 10.4461/ GFDQ.2018.41.9

34. Vecchio A.; Anzidei M.; Serpelloni E.; Florindo F. Natural Variability and Vertical Land Motion Contributions in the Mediterranean Sea-Level Records over the Last Two Centuries and Projections for 2100. Water, **2019**, 11, 148

35. Ravanelli, R.; Riguzzi, F.; Anzidei, M.; Vecchio, A.; Nigro, L.; Spagnoli, F.; Crespi, M. Sea level rise scenario for 2100 AD for the archaeological site of Motya. Rendiconti Lincei. Scienze Fisiche e Naturali. https://doi.org/10.1007/s12210-019-00835-3

36. Anzidei, M.; Lambeck, K.; Antonioli, F.; Furlani, S.; Mastronuzzi, G.; Serpelloni, E. and Vannucci, G. Coastal structure, sea-level changes and vertical motion of the land in the Mediterranean. *Geol. Soc. Lond. Spec. Publ.* **2014b**, 388(1):453–479. https ://doi.org/10.1144/SP388 .20

37. Reimann, L.; Vafeidis, A.T.; Brown, S.; Hinkel, J.; Tol, R.S.J. Mediterranean UNESCO World Heritage at risk from coastal flooding and erosion due to sea-level rise. *Nature Comm.* **2018**, 9:4161, DOI: 10.1038/s41467-018-06645-9

38. Rovere, A.; Antonioli, F.; Enei, F.; Giorgi, S. Relative sea level change at the archaeological site of Pyrgi (Santa Severa, Rome) during the last seven millennia. Quaternary International, 2011, 232, 82-91.

39. Masselink, G.; Hughes, M.G. Introduction to Coastal Processes and Geomorphology. Edward Arnold, London, 354 pp. McCann, S.B. (ed.) 1980.

Preprints (www.preprints.org) | NOT PEER-REVIEWED | Posted: 17 October 2019 doi:10.20944/preprints201910.0202.v1

Figures

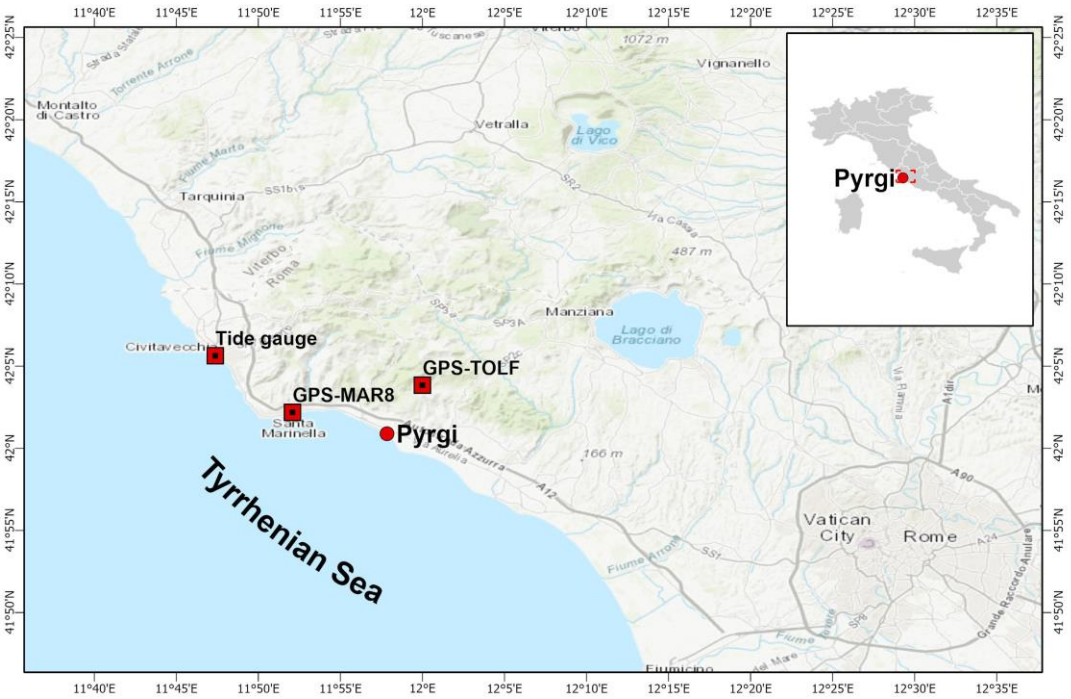

Fig.1 The investigated area of Pyrgi with the location of the CGPS stations of MAR8 and TOLF and the nearby tide gauge station of Civitavecchia.

Fig.2 The orthophoto with the Ground Control Points (red dots) position used during the UAV surveys.

Preprints (www.preprints.org) | NOT PEER-REVIEWED | Posted: 17 October 2019 doi:10.20944/preprints201910.0202.v1

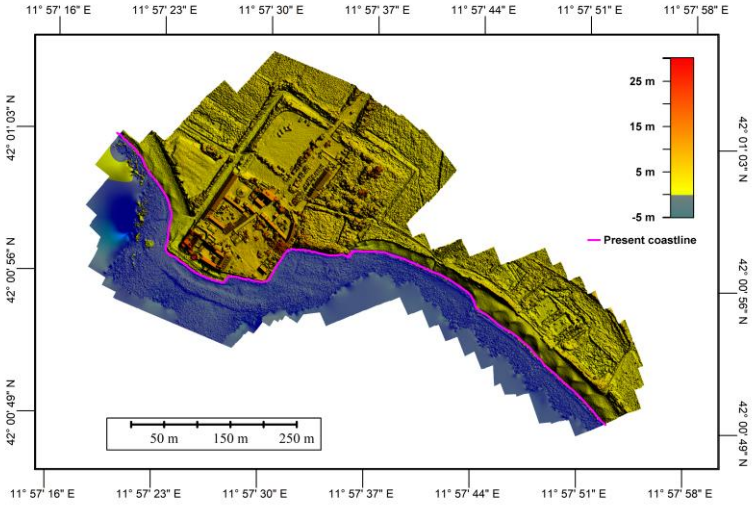

Fig.3 The Digital Surface Model (DSM) of the coastal sector of Pyrgi, from the analysis of the aerial photos.

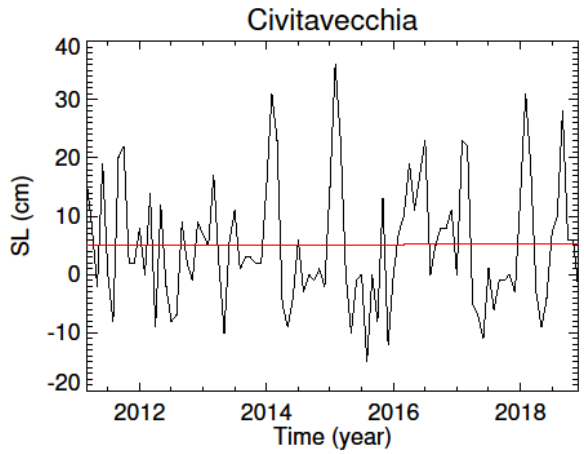

Fig.4 a

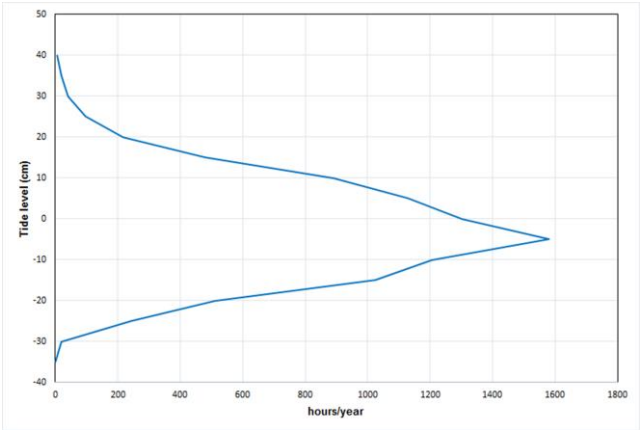

Fig.4 b

Fig.4. a) The sea level recordings at the tide gauge of Civitavecchia, for the time span 2011-2019 (about 9 years), located nearby Pyrgi (see Fig.1 for location). In b) is the Statistical diagrams of tide gauges data of height (cm) tide trend (hours/year) of the analyzed tide gauge of Civitavecchia.

Preprints (www.preprints.org) | NOT PEER-REVIEWED | Posted: 17 October 2019 doi:10.20944/preprints201910.0202.v1

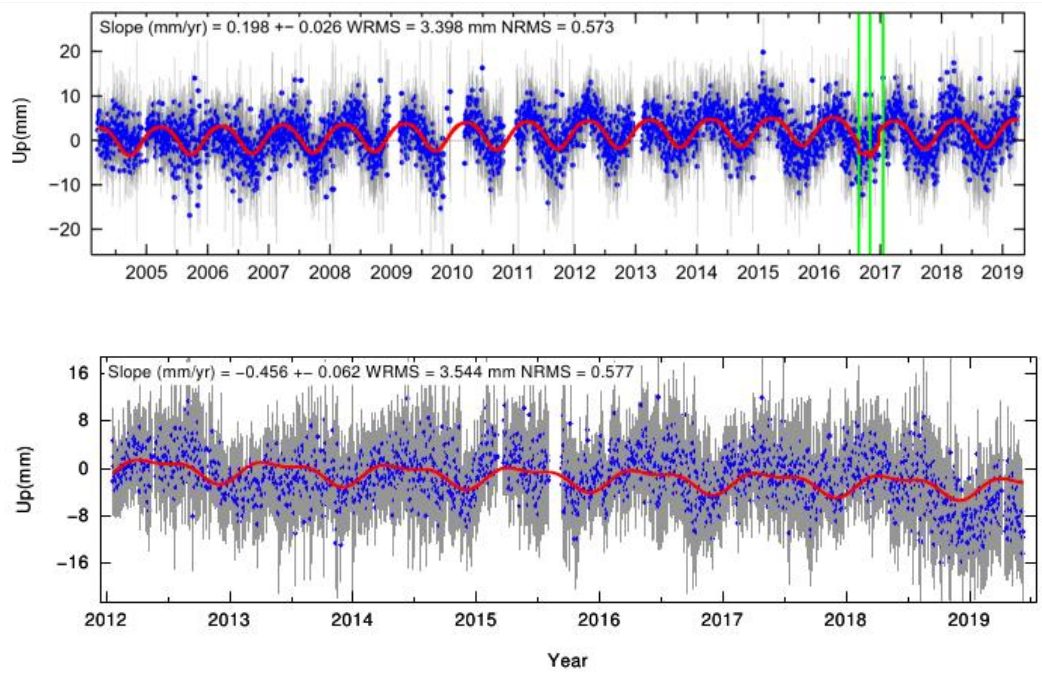

Fig.5. The UP time series of the GNSS station for a) TOLF (time span 2004-2019, about 15 years) and b) MAR8 (time span 2012-2019), both located nearby Pyrgi (see Fig.1 for location).

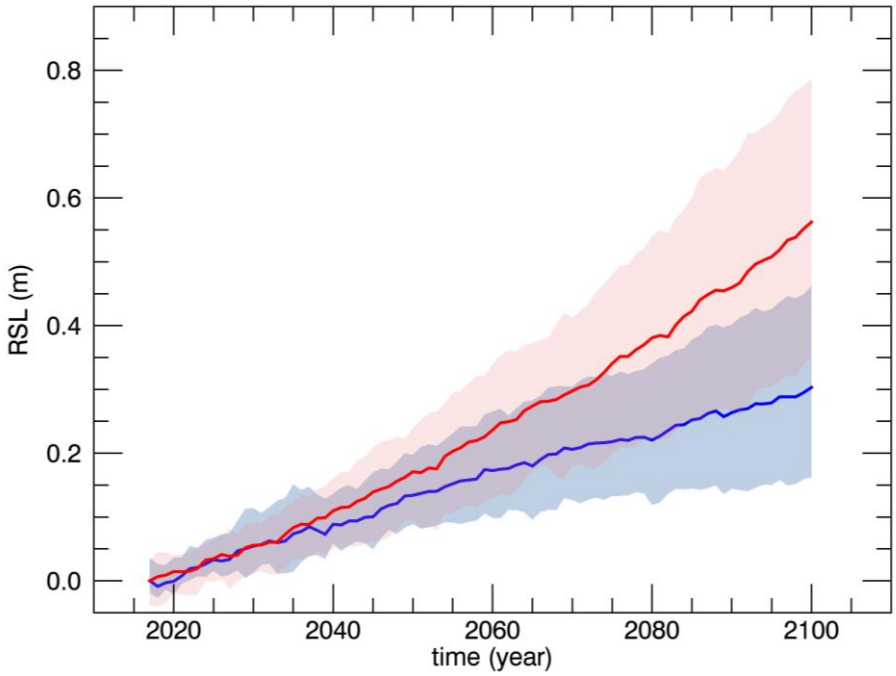

Fig. 6 Relative sea level with respect to the 2017 level as obtained from the regional IPCC sea-level projections, AR5 RCP2.6 (blue line) and RCP8.5 (red line) for a null VLM. Color bands represent the 90% confidence interval. The small-scale variations observed in the data are related to the ocean component contribution accounting for the effects of dynamic SSH, the global thermosteric SSH anomaly and inverse barometer effects (Church et al., 2013a, b; http://icdc.cen.unihamburg.de/).

Preprints (www.preprints.org) | NOT PEER-REVIEWED | Posted: 17 October 2019 doi:10.20944/preprints201910.0202.v1

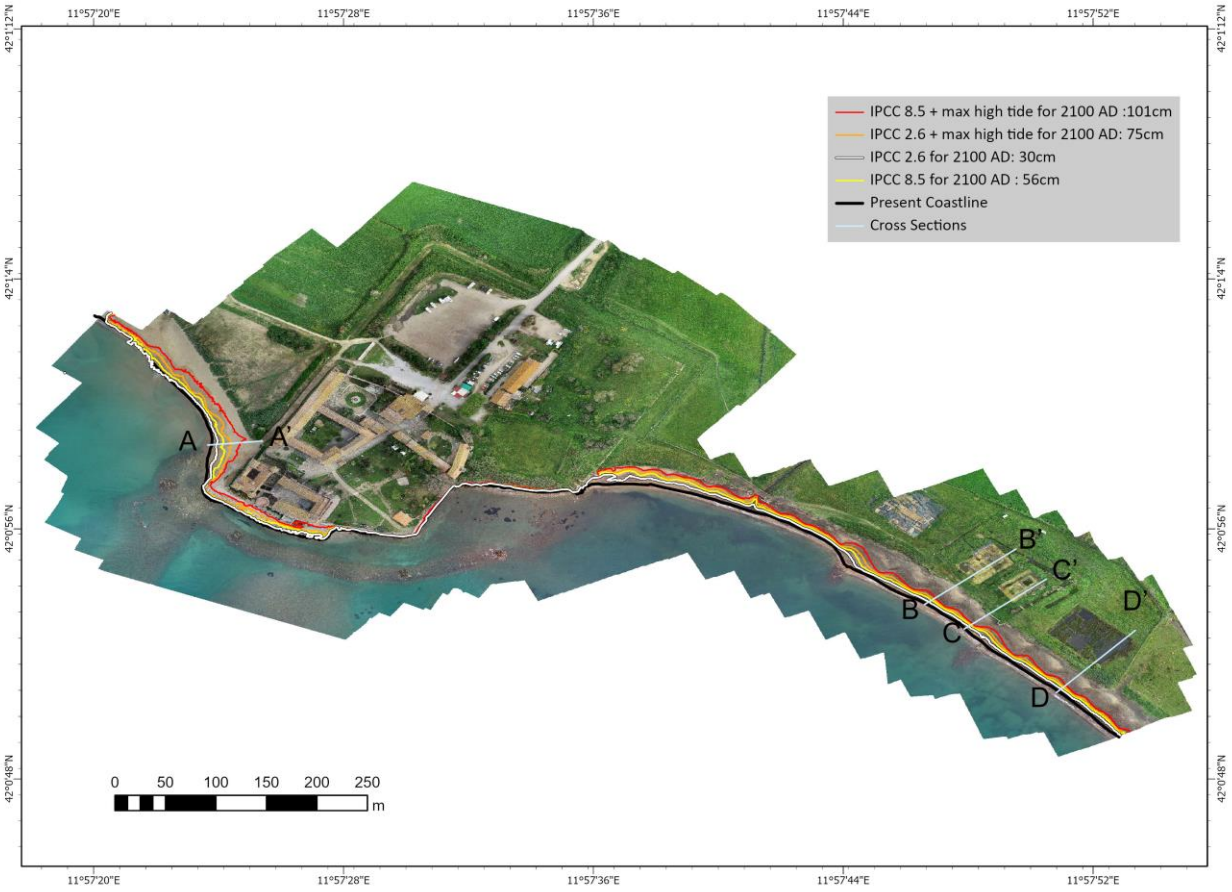

Fig. 7 Projected coastline positions for 2100 A.D. for the 2.6 and 8.5 IPCC scenarios (see legend for details). The cross sections along the shore are also shown in the figure.

Preprints (www.preprints.org) | NOT PEER-REVIEWED | Posted: 17 October 2019 doi:10.20944/preprints201910.0202.v1

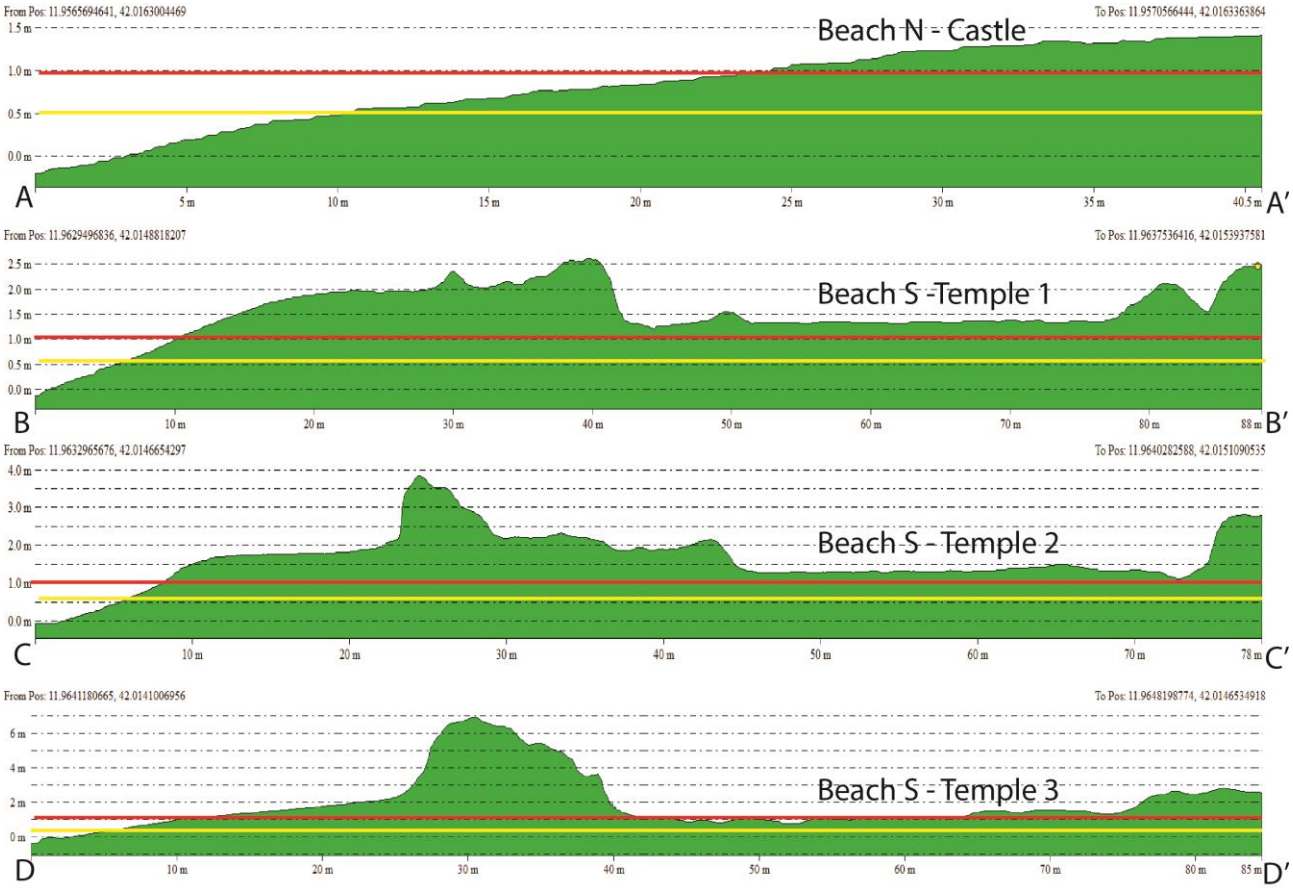

Fig.8 Cross sections of the coastline. See also Fig. 7 for cross section positions. A-A' north of the castle of Santa Severa; B-B', C-C' and D-D' across the beach and the three structures of the temple of Pyrgi. The expected sea levels for 2100 in the RCP8.5 scenario and in the maximum RCP8.5 high tide condition, are shown by the yellow and red lines, respectively.

Tables

Survey and Camera features			
Number of images	306	Camera stations	286
Flying altitude	79.8 m	Tie points:	1,158,646
Ground resolution	1.94 cm/pix	Projections:	3,891,753
Coverage area:	0.226 km²	Reprojection error	0.528 pix
Camera Model	FC6310 (8.8mm)	Focal Length	8.8 mm
Camera Resolution	5472 x 3648	Pixel Size	2.41 x 2.41 µm

Tab.1. Survey features

Preprints (www.preprints.org) | NOT PEER-REVIEWED | Posted: 17 October 2019 doi:10.20944/preprints201910.0202.v1

Sea level 2050 IPCC 8.5 (cm)			*Sea level 2050 IPCC 2.6 (cm)*		
RSLR	RSLR + Mean high tide (30 cm)	RSLR + Max high tide (45 cm)	RSLR	RSLR + Mean high tide (30 cm)	RSLR + Max high tide (45 cm)
17±0.07	**47**	**62**	**13**	**43**	**58**
Sea level 2100 IPCC 8.5 (cm)			*Sea level 2100 IPCC 2.6 (cm)*		
RSLR	RSLR + Mean high tide (30 cm)	RSLR + Max high tide (45 cm)	RSLR	RSLR + Mean high tide (30 cm)	RSLR + Max high tide (45 cm)
56±0.22	**86**	**101**	**30**	**60**	**75**

Tab.2 Relative Sea Level Rise (cm) above the current mean sea level at Pyrgi for 2050 and 2100 for the IPCC 2.6 and 8.5 climatic scenarios, in the mean and maximum high tide conditions.

IPCC scenario	*RSLR 2100 (cm)*	*Land loss (m^2)*	*% of land loss* (16113.55 m^2)
IPCC 2.6	17±0.07	2033.33	12.6
IPCC 2.6 + max high tide	75±0.22	5387.87	33.4
IPCC 8.5	56±0.22	3790.47	23.5
IPCC 8.5 + max high tide	101±0.22	7480.02	46.4

Tab.3. IPCC scenarios, relative sea level rise projections for 2100, expected land loss (m^2) and percentage of land loss with respect to the current surface for the given RSLR projections.